Dynamic Pathways for Fluxional Molecules Defined Using Exchange-NOE Peaks

Enzo Alessio,[‡] Lory Hansen,[†] Marian Iwamoto,[†] and Luigi G. Marzilli*[,†]

Contribution from the Department of Chemistry, Emory University, Atlanta, Georgia 30322, and the Dipartimento di Scienze Chimiche, Università di Trieste, 34127 Trieste, Italy

Received February 5, 1996[⊗]

Abstract: In examining NMR methods to assess orientation and fluxional motions of planar N-donor heterocyclic coordinated ligands (L's) in solution, we introduce the use of exchange-NOE NMR data as a powerful method for defining (i) the extent of L rotation about the metal-N bond, (ii) the direction of L rotation, and (iii) even the halves of C_2-symmetrical L's that interchange during dynamic processes. The full value of the approach depends on a strategy in which the complexes studied are chiral and similar except that one has a lopsided L (Me_3Bzm = 1,5,6-trimethylbenzimidazole in $[Re_2O_3Cl_4(Me_3Bzm)_4]$ (**1**)) and the other has a C_2-symmetrical L (3,5-lut = 3,5-lutidine in $[Re_2O_3Cl_4(3,5\text{-lut})_4]$ (**2**)). Each Re is part of a nearly linear O═Re−O−Re═O grouping and has a "terminal" L (L^t) and a stacked L (L^s). The fluxional inversion of the two chiral dimers involves rotations of ∼180° about the Re−O−Re bonds and of ∼90° about all four Re−L bonds. The exchange-NOE data for **2** show that the half of L^t away from the dimer center interchanges with the half of L^s close to the center, with the L plane rotating past the O═Re−O bonds, not the N−Re−Cl bonds. Thus, the exchange-NOE data help to establish the direction of L rotation. In **1**, Me_3Bzm^t has the rare head-to-head (HH) orientation with respect to the partner. This partner Me_3Bzm^s stacks with the Me_3Bzm^s from the other Re in the common head-to-tail (HT) orientation. Compelling evidence that the predominant solution conformer of **1** has the HH,HT,HH structure includes unusual chemical shift dispersions and a strong interligand NOE cross-peak. This is the only case in which *cis*,*bis* imidazole-ring-ligated untethered ligands have been found to be predominantly HH in solution. This predominance can be attributed to the electrostatic attraction of the δ^+ N_2C proton for the negative core of the molecule (bridging O, *cis* Cl on same Re, and two *cis* Cl's on the other Re).

Introduction

A wealth of solid-state structural information from X-ray crystallography has enriched our knowledge of the chemistry of metal compounds. In contrast, the dynamic pathways and the solution structures of fluxional species are much less well understood. However, it is usually in solution that metal species act as catalysts, as reagents for organic synthesis, as active sites in metalloenzymes, etc. The multitude of potential dynamic pathways that octahedral mononuclear and polynuclear metal complexes possess, combined with a paucity of suitable experimental approaches, has limited our knowledge of these dynamic processes. Here we present a general strategy that has provided excellent insight into the dynamic and structural properties of fluxional complexes in solution. Our study also reveals a feature of the coordinated imidazole ring that seems likely to influence the biological role of imidazole rings in many metallobiochemicals.

This study arose from an initial objective directed at understanding the factors influencing the orientations and dynamic motions of *cis* coordinated nucleopurines. These properties in metalloanticancer drug DNA adducts influence the nature of the adducts formed and the activity of the adducts. Nucleopurines, like other important N-donor heterocyclic bioligands, possess a plane of symmetry passing through the rings, but they are lopsided, i.e., they lack C_2-symmetry. Metalloproteins or enzymes in which the metal has two coordinated heterocyclic lopsided imidazole ligands are almost ubiquitous.[1]

Nucleobases have relatively few nonexchangeable protons, and their orientation in solution is difficult to define by NMR spectroscopy. To circumvent this limitation, we have been using the nucleopurine analog, 1,5,6-trimethylbenzimidazole (Me_3-Bzm, Chart 1). This ligand has the very useful characteristic of having protons distributed around the entire molecule; each proton has a singlet NMR signal.[2] Like nucleopurines, Me_3-Bzm is a five-six bicyclic system but the six-membered ring lacks an exocyclic group directed toward the *cis* coordinated ligands. This difference in steric properties is helpful in assessing the contributions of steric effects to structural changes in DNA when metal species, such as metal anticancer agents, are bound to DNA. Finally, Me_3Bzm is also of particular interest in B_{12} model chemistry.[3] For two *cis* lopsided N-heterocyclic ligands (B, e.g., purines), the corresponding atoms of each B can be on the same or opposite sides of the N−M−N plane, giving the head-to-head (HH) and the head-to-tail (HT) orientations, respectively. In a preliminary communication, we described the rarity of finding the HH orientation of two *cis* lopsided ligands.[2] A HT arrangement is the most common solid-state conformation of *cis*-bis(ligand) complexes of purines with Pt^{II}, Co^{III}, Cu^{II}, and Zn^{II} metal centers.[4] Only four HH solid-state structures of untethered ligands had been reported, all of which are square-planar Pt^{II} complexes with 9-ethylguanine,[5] until our recent brief report on the dynamic properties and stereochemistry of Ru− and Re−Me_3Bzm complexes.[2] For one of these rare HH species, $Re_2O_3Cl_4(Me_3Bzm)_4$ (**1**), only a figure of the structure was shown.[2] Our analysis of new results on this and related Re species has led to the identification of some interesting and important new phenomena which are likely to

[†] Emory University.
[‡] Università di Trieste.
[⊗] Abstract published in *Advance ACS Abstracts,* August 1, 1996.

(1) Lippard, S. J.; Berg, J. M. *Principles of Bioinorganic Chemistry*; University Science Books: Mill Valley, CA, 1994.
(2) Marzilli, L. G.; Iwamoto, M.; Alessio, E.; Hansen, L.; Calligaris, M. *J. Am. Chem. Soc.* **1994**, *116*, 815−816.
(3) Charland, J.-P.; Zangrando, E.; Bresciani-Pahor, N.; Randaccio, L.; Marzilli, L. G. *Inorg. Chem.* **1993**, *32*, 4256−67.
(4) Xu, Y.; Natile, G.; Intini, F. P.; Marzilli, L. G. *J. Am. Chem. Soc.* **1990**, *112*, 8177−9, and references therein.
(5) Schöllhorn, H.; Raudaschl-Sieber, G.; Müller, G.; Thewalt, U.; Lippert, B. *J. Am. Chem. Soc.* **1985**, *107*, 5932−7, and references therein.

S0002-7863(96)00385-X CCC: $12.00

Chart 1. NMR Labeling Scheme for the Me_3Bzm Ligand[a]

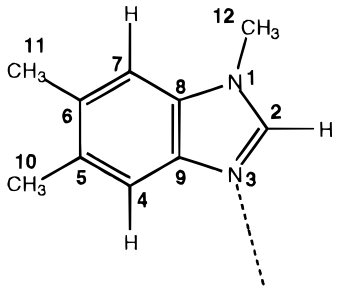

[a] The carbons are designated as "B" which refers to the benzimidazole ring.

Table 1. Crystallographic Data for $Re_2O_3Cl_4(Me_3Bzm)_4 \cdot 2(CH_3)_2CO$

chemical formula	$C_{46}H_{60}Cl_4N_8O_5Re_2$
formula weight	1319.2
space group	*C*2/*c*
Z	8
a (Å)	35.020(12)
b (Å)	16.308(5)
c (Å)	25.507(7)
β (deg)	132.870(0)
V (Å^3)	10676(8)
ρ_{calcd} (g/cm^3)	1.64
λ (Å)	0.71073 (Mo Kα)
μ (mm^{-1})	4.84
T (K)	173
scan technique	ω
transm coeff (%)	4.7−11.9
R (%)	5.62
R_w (%)	6.43
goodness-of-fit	1.43

be significant in areas beyond those which motivated our study. Furthermore, our study shows the power of the interpretation of exchange-NOEs in providing insight into the dynamic motions of molecules.

Experimental Section

$Re_2O_3Cl_4(Me_3Bzm)_4$ (1). A solution of Me_3Bzm (0.26 g, 1.6 mmol)[3] in acetone (20 mL containing 10 μL of H_2O) was added dropwise to a stirred suspension of $ReOCl_3(Me_2S)(OPPh_3)$[6] (0.325 g, 0.5 mmol) in acetone (30 mL). The mixture was left at room temperature overnight. The emerald-green solution obtained after filtration of a white precipitate ($Me_3Bzm \cdot HCl$) was concentrated to ~15 mL and refrigerated. A deep-green crystalline precipitate, formed within 2 days, was collected, washed with water, cold acetone, and diethyl ether, and then vacuum dried: yield 0.18 g (60%). Anal. Calcd for $C_{40}H_{48}Cl_4N_8O_3Re_2$ (M_w 1203.09): C, 39.93; H, 4.02; N, 9.31; Cl, 11.78. Found: C, 39.90; H, 4.06; N, 9.22; Cl, 11.86. The complex (0.12 g) was recrystallized from dimethylformamide (DMF)/acetone mixtures (0.9 mL/6 mL) by addition of diethyl ether. The crystals contain acetone (by NMR) but desolvate readily and could not be analyzed: yield 65%.

$Re_2O_3Cl_4(3,5\text{-lut})_4$ (2) (lut = lutidine). **2** was prepared by the method used for **1**. The clear emerald-green solution was concentrated to ~10 mL and then refrigerated. A deep-green precipitate formed in a few hours and was collected in 72% yield and dried as above. Anal. Calcd for $C_{28}H_{36}Cl_4N_4O_3Re_2$ (M_w 990.84): C, 33.94; H, 3.66; N, 5.65; Cl, 14.31. Found: C, 34.16; H, 3.78; N, 5.55; Cl, 14.21.

X-ray Crystallography. Crystal data and refinement parameters are summarized in Table 1. A green crystal of $Re_2O_3Cl_4(Me_3Bzm)_4 \cdot 2CH_3COCH_3$ (**1**) was mounted on a glass fiber, placed on a Siemens P4 diffractometer, and cooled to −100 °C with a LT2 low-temperature device to prevent crystal decay. Crystals of **1** desolvate within 20 min when removed from the mother liquor at room temperature. The crystal system for **1** was determined by automatic indexing of 38 centered reflections. Refined cell constants were obtained by least-squares refinement of 15 of the high-angle reflections ($17° < 2\theta < 44°$). Intensities were collected using monochromated Mo Kα radiation (λ = 0.71073 Å). Three check reflections were measured every 97 reflections; there was no significant deviation in intensity. Intensities were corrected for Lorentz and monochromator polarization effects and absorption (semiempirical method based on azimuthal scans). Systematic absences were consistent with space groups *C*2/*c* (centrosymmetric) and *Cc* (noncentrosymmetric). The space group *C*2/*c* was selected on the basis of the statistical distribution of intensities (mean $|E^2 - 1| = 1.030$). The structure was solved by Patterson methods and refined by full-matrix least-squares procedures using SHELXTL PLUS (VMS). The acetone molecules in **1** were highly disordered and were refined isotropically as rigid groups pivoting about the central carbon atoms (C41, C44) with idealized bond lengths (d(C−O) = 1.302 Å, d(C−C) = 1.540 Å) and bond angles (120°). All other non-hydrogen atoms were refined anisotropically. H-atoms were included at calculated (d(C−H) = 0.96 Å) positions with isotropic thermal parameters fixed at 0.08.

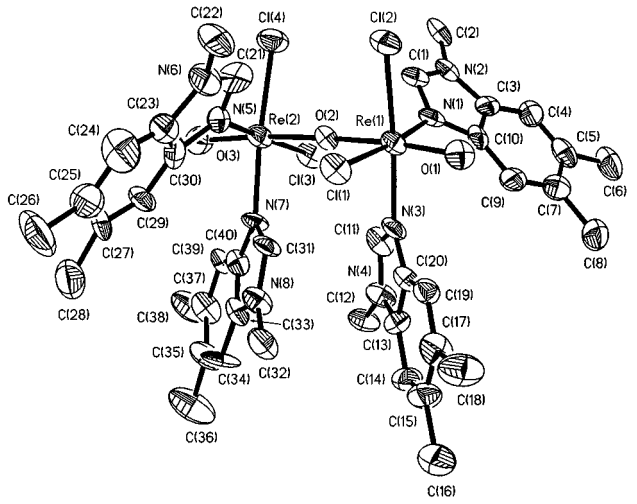

Figure 1. Perspective drawing of $Re_2O_3Cl_4(Me_3Bzm)_4$ (**1**) with 50% probability for the thermal ellipsoids.

NMR Spectroscopy. NMR spectrometers used were JEOL EX400 and General Electric QE-300, NT-360, and GN-600 Omega models. Sample concentrations were ~50 mM. All spectra were referenced to TMS unless otherwise noted. ^{1}H 1D data were collected typically with a 3600−7200 Hz window, a 30° pulse width, and 16K data points. Variable temperature (VT) 2D NOESY/EXSY spectra were recorded on the JEOL instrument. 2D parameters include: matrix of 512 × 1024; the second dimension was zero filled to 1024 data points prior to Fourier transformation; eight scans per t_1 increment were preceded by two dummy scans, with a spectral window 3959 Hz, pulse delay of 2.37 s, a mixing time of 500 ms, and a square sine bell function with no phase shift applied in both dimensions.

Results

Structural Studies. A perspective drawing of the $Re_2O_3Cl_4(Me_3Bzm)_4$ (**1**) structure appears in Figure 1. As in the py (pyridine) analogue, $Re_2O_3Cl_4(py)_4$ (**3**),[7] the nitrogen donor ligands on each pseudo-octahedral Re atom are *cis* to each other, and the molecule has a pseudo two-fold axis through the bridging oxo ligand, O(2). The most interesting features of the molecule are the HH arrangement of the two *cis* Me_3Bzm ligands on each Re (the "Re-ligand-partners") and the extended network of four Me_3Bzm ligands. The center of the network has two HT pseudo-bridging "stacked" Me_3Bzm's, designated as Me_3Bzm^s. The Re-ligand-partner of each Me_3Bzm^s is designated Me_3Bzm^t for "terminal".

In discussing the Me_3Bzm parameters, we use the numbers in Chart 1 and refer to carbons as B2, etc. All four Re−N−B2 bond angles (supporting information) are consistently more acute than the four Re−N−B9 bond angles. Unsymmetrical angles are common in Co^{III} complexes with Me_3Bzm: Co−N−B2

(6) Grove, D. E.; Wilkinson, G. *J. Chem. Soc. A* **1966**, 1224−30.

(7) Lock, C. J. L.; Turner, G. *Can. J. Chem.* **1977**, *55*, 333−9.

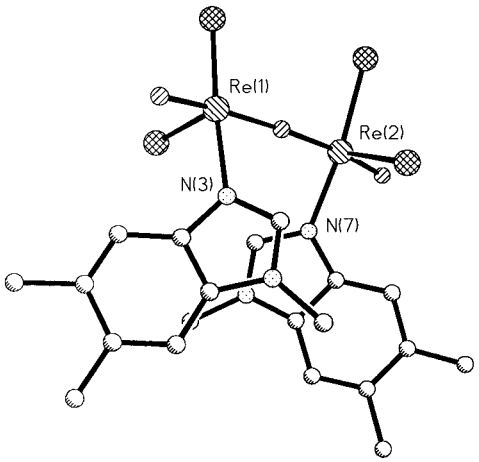

Figure 2. Perspective view of the intramolecular stacking interaction between the Me_3Bzm^s ligands for $Re_2O_3Cl_4(Me_3Bzm)_4$ (**1**). The two Me_3Bzm^t ligands are omitted for clarity.

angles range 121.1(3)−123.1(2)°; Co−N−B9 angles range 132.3(3)−133.7(2)°.[3,8−10]

The Me_3Bzm ligands in **1** are rotated about the Re−N bond 34−54° away from coplanarity with the plane defined by Re and the *cis* Cl atoms. In addition, the two halves of the dimer are rotated about the Re(1)−Re(2) vector away from an eclipsed conformation. Treating the Re−Re vector as a "bond", we find that a N(3)−Re(1)−Re(2)−N(7) "torsion angle" of 28° results from the greater overlap of the Me_3Bzm^s ligands (Figure 2). The shortest interplanar distance between the Me_3Bzm^s ligands is 3.1 Å. The two Me_3Bzm^t ligands are rotated ∼180° away from each other.

NMR Spectroscopy. The 1D and 2D ^{1}H NMR spectra of **1** and **2** (Figures 3−6) are consistent with both being fluxional molecules. At 20 °C, **1** has only six signals for the Me_3Bzm ligand, and these signals are somewhat broad, suggesting an exchange process with a rate at the fast end of the intermediate NMR time scale. For **2**, the signals are sharp, consistent with a faster exchange process. Spectra at lower temperature for **1** and **2** (Figures 3−6) show initial broadening of peaks. At very low temperatures, the spectra for both sharpen with the emergence of nearly twice the number of peaks apparent at room temperature. These results suggest that the molecules exist in solution with the N-heterocycle in two different environments and that the ligands interchange position between these environments relatively rapidly at ambient temperatures. Details of the NMR results are discussed below.

Discussion

Solid-State Structure. The interesting extended HH,HT,-HH arrangement of Me_3Bzm's in **1** (Figure 1) can be attributed in large part to the electrostatic attraction of the δ^+ H2's on Me_3Bzm^t's toward the negative O and Cl groups in the core of the dimer. There are several reasons why we believe this is the key interaction that dictates conformation. First, there are so many favorable interactions; for example, the δ^+ H on C(21) in Figure 1 is attracted by four negative groups, Cl(4), Cl(2), Cl(1), and O(2). Second, in a related dimer with one pyridine (py) and one Me_3Bzm on each Re, the py occupies the pseudo bridging site while the Me_3Bzm occupies the terminal site with the same orientation found in **1**.[11] Py lacks the very acidic H characteristic of the H2 in an imidazole ring. Finally, although

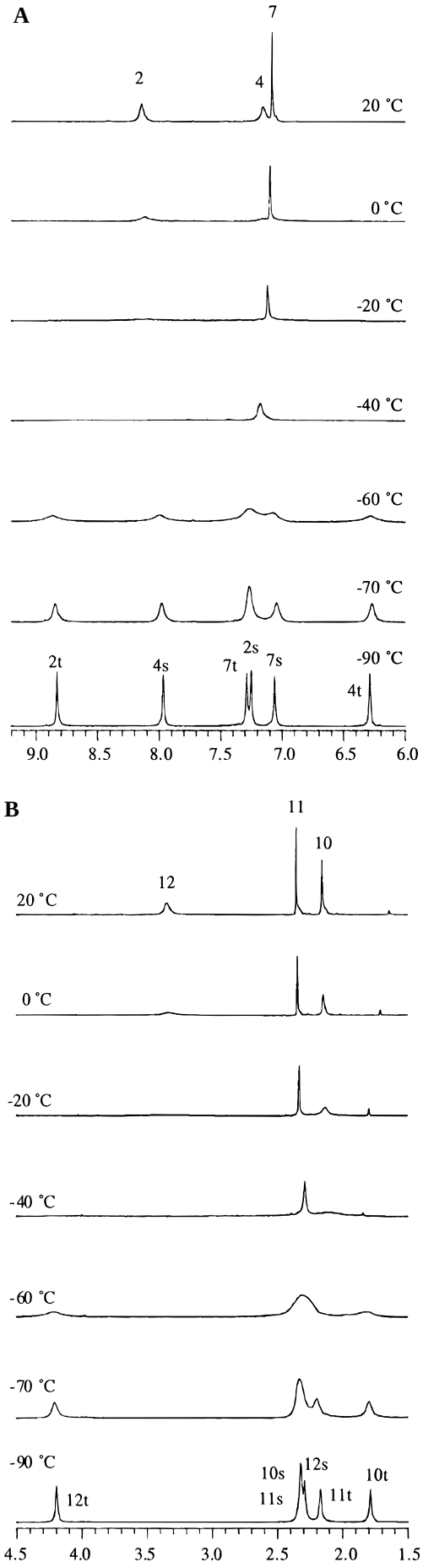

Figure 3. ^{1}H NMR spectra of $Re_2O_3Cl_4(Me_3Bzm)_4$ (**1**) in CD_2Cl_2 at various temperatures in the downfield (A) and upfield (B) regions. Signal assignments for the stacked and terminal Me_3Bzm are indicated.

(8) Yohannes, P. G.; Bresciani-Pahor, N.; Randaccio, L.; Zangrando, E.; Marzilli, L. G. *Inorg. Chem.* **1988**, *27*, 4738−44.
(9) Parker, W. O., Jr.; Zangrando, E.; Bresciani-Pahor, N.; Marzilli, P. A.; Randaccio, L.; Marzilli, L. G. *Inorg. Chem.* **1988**, *27*, 2170−80.
(10) Charland, J.-P.; Attia, W. M.; Randaccio, L.; Marzilli, L. G. *Organometallics* **1990**, *9*, 1367−75.
(11) Alessio, E.; Zangrando, E.; Marzilli, L. G. unpublished work.

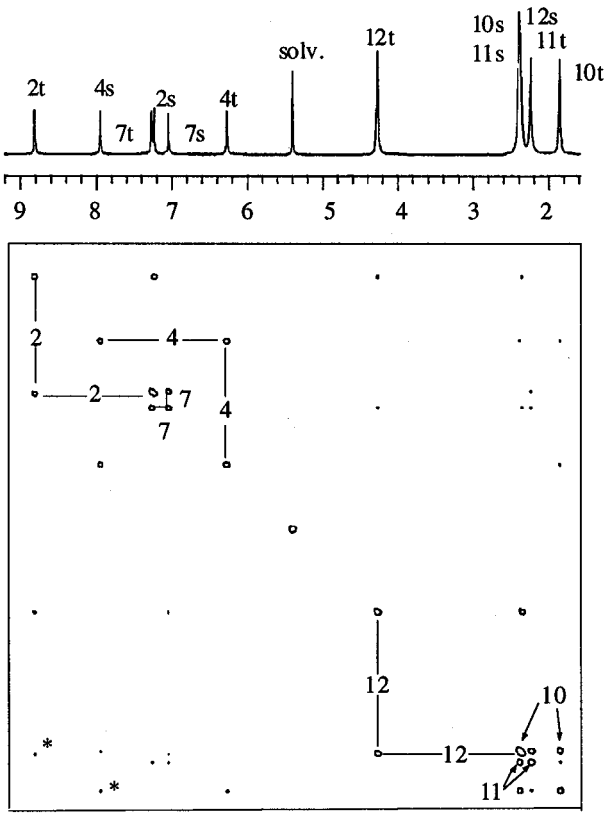

Figure 4. 2D ^{1}H NOESY/EXSY spectrum of **1** in CD_2Cl_2 at −90 °C. The exchange pathways are shown. Some exchange-NOE peaks are marked with an asterisk, for example, the 2t-12s exchange-NOE.

Re^V and Ru^{II} are very different metal centers, the relative stability of the atropisomers found for Ru^{II} complexes of lopsided ligands can best be rationalized by invoking this type of electrostatic attraction of the δ^+ H2 toward the coordinated Cl ligands.[12]

The distribution of negative groups surrounding the stacked site is more symmetrical than for the terminal site. In the observed Me_3Bzm^s orientation, the bulky Me_3Bzm^s six-membered ring is directed away from the bulkiest ligand on the same Re, Me_3Bzm^t. The lower steric crowding favors the observed HT Me_3Bzm^s orientation compared to the orientation obtained by rotation of Me_3Bzm^s by 180° from that in **1**. These steric and electrostatic factors act in concert to favor the HH,-HT,HH conformer observed in the solid.

Spectral Assignments and Solution State Structure. The spectral assignments and the assessment of the structure of **1** in CD_2Cl_2 depended on anisotropic shift arguments and on EXSY cross-peaks in the 2D NOESY/EXSY data at −90 °C (Figure 4). As background for our assignment, we first review our use of the anisotropic effects of one Me_3Bzm on the shifts of the signals of the other Me_3Bzm to assign signals and determine the relative Me_3Bzm orientations of *cis,cis,cis*-$RuCl_2(Me_2SO)_2(Me_3Bzm)_2$.[2] The anisotropic effects were greatest on the H2 and H4 signals. In the canted orientation adopted by HH species, H2 of one Me_3Bzm is pointed toward the other Me_3Bzm and H4 of this other Me_3Bzm is pointed toward the first Me_3Bzm. As a result, a characteristic up/downfield set of H2 and of H4 signals is produced. Since H7 of both Me_3Bzm points away from the coordination sphere, the anisotropic effects on this signal were too small to aid structure elucidation; the H7 assignments depended on NOE data. The NOE patterns readily allowed signal assignments since the Me_3-Bzm ligands occupy distinct sites in the Ru^{II} complex and do not interchange position.

(12) Alessio, E.; Calligaris, M.; Iwamoto, M.; Marzilli, L. G. *Inorg. Chem.* **1996**, *35*, 2538−2545.

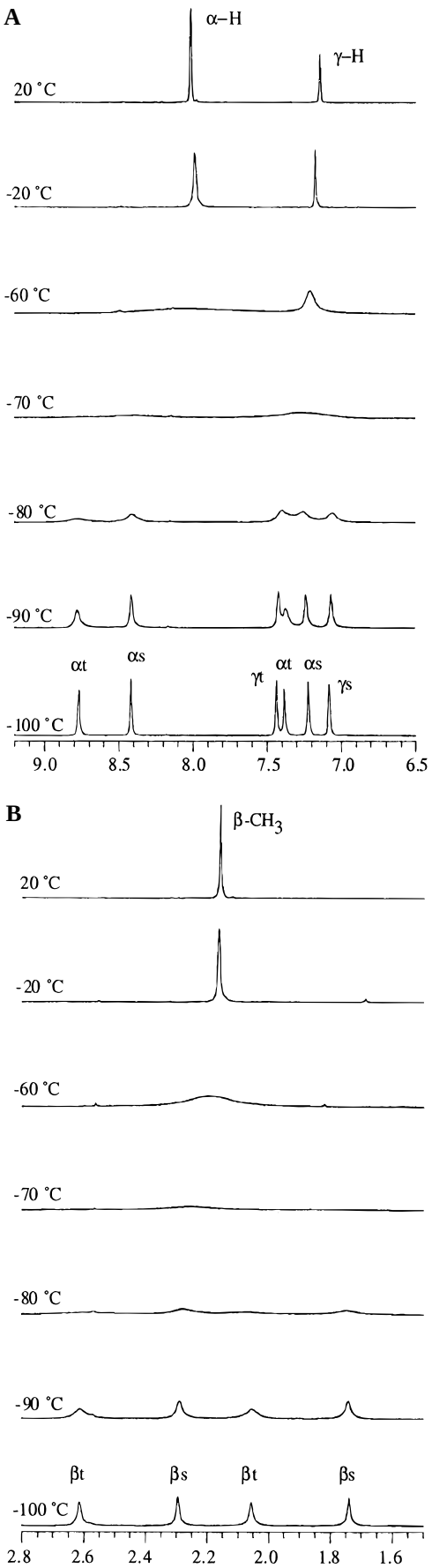

Figure 5. ^{1}H NMR spectra of $Re_2O_3Cl_4(3,5\text{-lut})_4$ (**2**) in CD_2Cl_2 at various temperatures in the downfield (A) and upfield (B) regions. Signal assignments for the stacked and terminal 3,5-lut are indicated.

The Me_3Bzm interchange between positions in **1** makes the 2D assignment procedure more difficult than for the Ru compound. We made an initial assumption that the conforma-

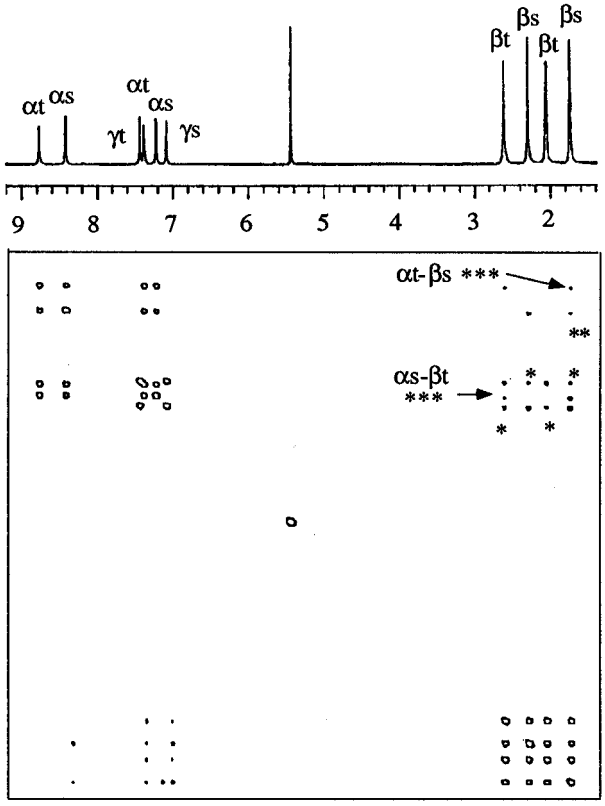

Figure 6. 2D ^{1}H NOESY/EXSY spectrum of **2** in CD_2Cl_2 at −100 °C. Since the combined rotations around Re−O and Re−N bonds will exchange all signals of a given type, for each α-H and β-CH_3 signal, there are three exchange cross-peaks to the other three α-H and β-CH_3 signals, respectively. The γ-H signals exchange also. These cross-peaks are close to the diagonal. Cross-peaks far from the diagonal are between β-CH_3 and α-/γ-H signals and are shown at two levels. The lower left of the figure (at a higher cut) shows only direct NOEs from β-CH_3 to α-H or γ-H signals. Higher cuts allowed assignments and allowed us to identify the direct NOEs. In the upper right (an intermediate contour), there are exchange-NOE peaks from β-CH_3 to γ-H (class i, *) and α-H (class ii, **) signals marked with asterisks. However, there are two other exchange-NOEs (class iii, ***). These are from the upfield α-H signal of the 3,5-lut^s to the downfield β-CH_3 signal of 3,5-lut^t and from the downfield α-H signal of 3,5-lut^t to the upfield β-CH_3 signal of 3,5-lut^s.

tion of **1** in the crystal also exists in solution at low temperature, except of course that **1** will have true C_2 symmetry and thus is chiral. We considered alternative structures, but only our initial assumption was totally consistent with all the NMR data.

In the assignments at −90 °C (Table 2), signals are labeled by the position of the proton and the type of Me_3Bzm. The first step in the assignment was to link protons of a given type in the two Me_3Bzm's using the EXSY peaks, which are very clear and the only peaks present at the highest contours that contain cross-peaks. The pattern, two pairs of one upfield and one downfield exchanging aromatic signals, is characteristic of B4H and B2H signals of an HH species.[2] No HT species is known to give this pattern. We assign the most downfield signal as 2t, the signal of B2H in Me_3Bzm^t. B2H is ordinarily the most downfield Me_3Bzm signal, and B2H in Me_3Bzm^t is far from the shielding region of the anisotropic Me_3Bzm^s. 2t has an EXSY peak to the upfield 2s, thus assigning it. In the other well-dispersed EXSY pair, the far upfield shifted signal must be 4t since B4H of Me_3Bzm^t is directed toward the shielding region of Me_3Bzm^s.

As expected on the basis of the HH structure, the most downfield methyl signal is assigned to 12t, since the $B12H_3$ group of Me_3Bzm^t is attached to a nitrogen and is directed away from the shielding region of the Me_3Bzm^s. The upfield EXSY partner ($B12H_3$ on Me_3Bzm^s directed toward the shielding region of Me_3Bzm^t) is usually found at ∼3.3 ppm (∼0.5 ppm from the typical shift of a coordinated Me_3Bzm).[2] However, the 12s signal is at 2.37 ppm, ∼1 ppm *even further upfield*. This unusual additional upfield shift can be explained readily with the HH,HT,HH structure. Each Me_3Bzm^s $B12H_3$ group lies over and is shielded by the six-membered ring of the C_2-related Me_3Bzm^s on the other Re of the dimer (Figure 2). The most upfield signal is 10t since the $B10H_3$ group of Me_3Bzm^t lies somewhat over Me_3Bzm^s. Thus, the NMR shift data are totally consistent with the same structure for **1** in the solid and solution states, except that a more symmetrical version exists in solution.

Next we used the 2D data to confirm the assignments based on shift arguments and to assign the signals with relatively small dispersion between the two types of Me_3Bzm. The NOESY/EXSY spectra of **1** (see Figure 4) have three types of cross-peaks. The first type, EXSY cross-peaks found at high contours and generally in the vicinity of the diagonal, was mentioned above as resulting from the physical exchange of the same Me_3Bzm between the stacked and the terminal sites. The other two types are smaller and generally far from the diagonal. The second type is a direct NOE, e.g., 4t-10t. The third type, an exchange-NOE, results from direct NOE interactions followed by physical exchange of the ligands between the two types of sites, e.g., 4s-10t. This exchange-NOE information is useful for gaining a deeper understanding of the pathways for exchange in **2**, see below.

The 2D data for **1** are somewhat complicated. First, the t-t NOE cross-peaks are generally stronger than the s-s cross-peaks. This may be due to differences in correlation times for the different parts of the molecule. Second, the 11s and 10s signals overlap. The complete assignment required analysis of peak intensities at several mixing times (150, 300, and 500 ms) and depended primarily on the better resolved t signals. At the 150 ms mixing time, the direct NOEs are most clearly identified. There are clear t-t NOE cross-peaks linking adjacent groups, 4t-10t-11t-7t-12t-2t. The NOE data allow confirmation of the assignments from shift arguments and the assignment of the two less dispersed signals, 11t and 7t. The t-s EXSY peaks allowed assignment of the s signals.

All the t-t NOE cross-peaks, except for 7t-12t, appear before any s-s NOE cross-peaks. As can be seen from Chart 1, the intraligand H7 to $B12H_3$ distance is relatively large since these protons reside on different rings. Thus the intraligand 7 to 12 NOE should be smaller than the other NOEs, accounting for the weak 7t-12t NOE. However, the 7s-12s NOE is one of the two strongest s-s cross-peaks. In the HT stacked arrangement, each Me_3Bzm^s H7 is close to *two* Me_3Bzm^s $B12H_3$ groups. Thus, the resulting two pathways for spin−spin interactions lead to a relatively large 7s-12s NOE cross-peak. The large 7s-12s NOE cross-peak strongly supports the conclusion from shift arguments that, in solution, **1** has the HH,HT,HH structure.

Since the exchange-NOE peaks result from a build-up of a direct-NOE followed by a dynamic process, they usually are seen most easily at longer mixing times. However, since the direct-NOEs also decay over time, and since there are many factors influencing the build-up and decay rates, it is not straightforward to treat the data quantitatively. At 500 ms, some exchange-NOE peaks can be observed at higher contour levels than the related direct-NOE peak. The relatively large 7s-12s NOE cross-peak leads to a 7s-12t exchange-NOE cross-peak that is larger than the direct 7t-12t NOE peak (Figure 4). Of the first eight non-EXSY peaks that we observe at the higher contours, one is an exchange-NOE at 150 ms but four are exchange-NOEs at 500 ms.

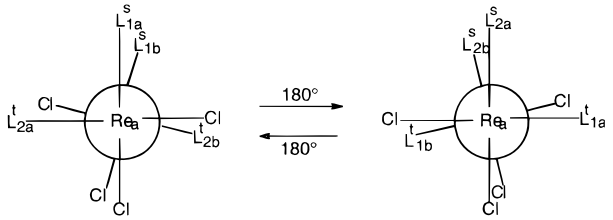

Figure 7. Schematic representation of the pairwise relationship of the L ligands during 180° net rotation about one Re−O bond (Re_b−O) in $Re_2O_3Cl_4L_4$ complexes. View is along the Re−O−Re bonds with Re_a obscuring Re_b. The pairs, (1a and 1b) and (2a and 2b), interchange between occupying both terminal sites and both stacked sites.

Dynamic Processes in $[ReOCl_2L^sL^t]O[ReOCl_2L^sL^t]$ Dimers. As mentioned, the ^{1}H NMR spectra of **1** and **2** at 20 °C indicate that both are dynamic. It is worthwhile to consider the general types of processes which can occur. The NMR data for **2**, discussed last, are particularly revealing and illustrate the power of using a combination of exchange-NOE information and C_2-symmetrical ligands to elucidate dynamic processes.

The types of dynamic processes that could be important are (a) rotation about the Re−N bonds and (b) rotation about the Re−O−Re bonds. The latter process is shown schematically in Figure 7. Combinations of (a) and (b) can occur. In order for the L^s and L^t signals to average, there must be rotation about the Re−O−Re bonds. This process must involve either two ∼90° rotations (one about each Re−O bond) or one ∼180° rotation about one Re−O bond. The 90° rotations could occur either stepwise or simultaneously. In either case, the L ligands can be seen to act in a pairwise fashion, unless there is bond breaking. Pair 1 (one L pair-mate on each Re) can together interchange position, both being either the L^s or the L^t type (Figure 7). Pair 2 (again one L pair-mate on each Re) can interchange likewise, always occupying the opposite type of position to pair 1. The pairwise relationship just described holds true even if the symmetry of an intermediate were to make the four ligands equivalent. The magnetic equivalence of protons does not mean they physically interchange; it means only that they interchange positions.

The overall dynamic process inverts the chirality of the dimer. The simple rotation of a net 180° around the Re−O−Re bonds converts the groupings L^s−Re−Cl and L^t−Re−Cl to L^t−Re−Cl and L^s−Re−Cl, respectively. It can be seen that the dimers in Figure 7 are mirror images of each other. The L ligand planes lie between the adjacent bonds, not along them. Such orientations are a component of the canting of one L toward the other. In **1**, H2 of Me_3Bzm^t lies along the direction of the plane approximately bisecting the bonds to the *cis* Cl and the *cis* bridging O, but H2 of Me_3Bzm^s has a similar relationship to the bonds to the *cis* Me_3Bzm^t and the *cis* bridging O. Thus, at some point during the inversion, each of the four Me_3Bzm's must also rotate by a net ∼90° about the Re−N bond (Figure 8).

Four types of Re−N rotations of 180° or less can be envisioned: clockwise by ∼90° and ∼180° or counterclockwise by ∼90° and ∼180°. We will show that the Re−N rotation process can be assessed with unprecedented insight by using the combined results from complexes with C_2-symmetrical ligands and from complexes with lopsided ligands.

Dynamic Processes in 1. The averaging of each type of Me_3Bzm signal for the two types of Me_3Bzm ligands of **1** at 20 °C (Figure 3) requires that rotation about the Re−O−Re bonds is rapid. However, the Me_3Bzm ligands could either rotate freely about the Re−N bonds or maintain a fixed orientation (*i.e.*, the Re-ligand-partners remain HH with each rotating by ∼90° during the inversion).

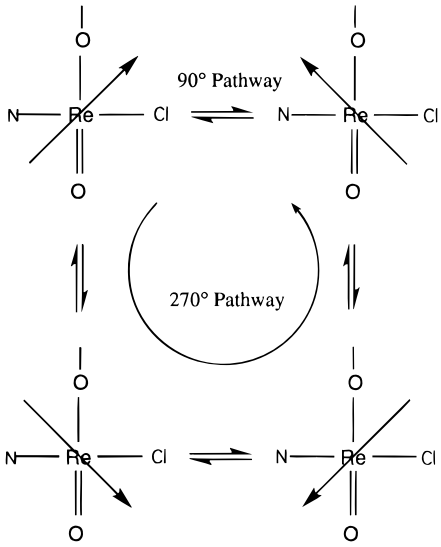

Figure 8. Schematic representation showing the relationship of the plane of a lopsided ligand (represented by the arrow) to the different CP and comparing the simple 90° rotation pathway to the more complicated 270° rotation pathway.

At lower temperature, broadening was observed for all resonances, including the sharper B7H and $B11H_3$ resonances (Figure 3). At −40 °C the B2H, B4H, $B12H_3$, and $B10H_3$ signals collapsed nearly into the baseline. As mentioned above, at lower temperature each signal split into two signals. Although slight changes in shift with temperature are common, the average shift of the two signals arising from each 20 °C signal was close to that of the unsplit signal. Since other conformations would not have the same distinctive pattern of shifts, the similarity of the shifts at low and high temperatures suggests that the major conformer of **1** has the HH,HT,HH structure regardless of temperature. Any intermediate species formed in the rotation process is likely to be unstable with respect to the ground state, since otherwise its signals would average with those of the major conformer and the observed shifts would be temperature dependent.

The EXSY peaks in the 2D spectrum (Figure 4) could arise solely from the inversion of chirality. Indeed, in contrast to the results with the 3,5-lut dimer (**2**, see below), the signals for the Me_3Bzm dimer are equally broadened at −60 to −70 °C. In the limit of slow exchange, signal broadening depends only on the rate constant for the process and not on the frequency difference between the exchanging signals.[13] The essentially equal broadening of the signals of both Me_3Bzm's indicates that the broadening of both sets is due to one rate-limiting exchange process.

In summary, all the NMR observations for **1** are consistent with (a) the presence of only one major conformer, (b) a HH,HT,HH structure for the major conformer, and (c) only one rate-limiting process.

Dynamic Processes in 2. For a *C_2-symmetrical ligand*, the exchange-NOE signals provide a high level of insight into dynamic processes. Furthermore, unlike the situation for lopsided ligands, the number of NMR signals expected depends on the extent of rotation about the M−N bonds (90° or 180°) and the rate of this process.

If rotation about the Re−O−Re bonds and the net 90° Re−N rotation accompanying inversion of chirality are rapid in $Re_2O_3Cl_4(3,5\text{-lut})_4$ (**2**), the signals expected for the C_2-symmetrical 3,5-lut ligand depend on the rate of the 180° rotation about the Re−N bonds. For very slow 180° rotation, 3,5-lut would give

(13) Sandström, J. *Dynamic NMR Spectroscopy*; Academic Press: London, 1982.

Table 2. Low-temperature ^{1}H NMR Assignments and Shifts for **1** and **2**[a]

$Re_2O_3Cl_4(Me_3Bzm)_4$ (**1**) at −90 °C			$Re_2O_3Cl_4(3,5\text{-lut})_4$ (**2**) at −100 °C		
	Me_3Bzm^t	Me_3Bzm^s		3,5-lut^t	3,5-lut^s
B2H	8.83	7.25	α-H[b]	7.38	7.22
B4H	6.29	7.96	β-CH_3[b]	2.05	1.73
B7H	7.28	7.05	γ-H	7.43	7.08
$B10H_3$	1.87	2.41	β-CH_3	2.61	2.29
$B11H_3$	2.25	2.41	α-H	8.77	8.41
$B12H_3$	4.28	2.37			

[a] CD_2Cl_2. [b] From parts of rings that are overlapped. Signals for 3,5-lut^t broad compared to those for 3,5-lut^s.

one γ-H, but two α-H and two β-CH_3 signals. For rapid 180° rotation, 3,5-lut would give one sharp signal for each proton type. Since the latter was found at room temperature (Figure 5), both 180° rotation about the Re−N bonds and the inversion of chirality are rapid.

On lowering the temperature, broadening is expected for the α-H and β-CH_3 signals but not for the γ-H signal, if only Re−N rotation is slowed. However, if dynamic inversion of the chirality is slowed, broadening is expected for the γ-H signal as well as the other signals. Therefore, the temperature dependence of the spectrum of **2** was studied. The ^{1}H NMR spectrum of **2** had a similar, although less pronounced, temperature dependence as the spectrum for **1**. A broadening of all peaks, including the γ-H signal, was observed below −40 °C (Figure 5). The broadening of the γ-H signal is indicative of slowing but continued dynamic inversion of the chirality of **2**, since 180° rotation about the Re−N bond will not influence the γ-H signal.

At still lower temperatures, e.g., −90 °C, there are clearly two sets of 3,5-lut signals, and each has two α-H and two β-CH_3 signals. This result indicates that the 180° Re−N rotation has also become slower. Also, the broadening of the two sets of 3,5-lut signals was not equal, indicating that one of the ligands was rotating more rapidly than the other. Thus **2** has two processes with rate-limiting steps of approximately the same time scale.

By tracing NOESY and EXSY cross-peaks in a 2D spectrum at −100 °C (Figure 6), we can readily identify the signals for each 3,5-lut. For each 3,5-lut, one half has upfield and one half has downfield α-H and β-CH_3 signals. One 3,5-lut has all its respective signals upfield to those of the other. In other words, the more upfield of the α-H signals of one is more upfield than the more upfield α-H signal of the other. The assignment is consistent with the temperature dependence of the ^{1}H NMR spectrum of **2**. This dependence allowed us to assign the signals to two sets because of the difference in broadening of each set; this difference is due to the differing rates of the 180° rotation process for each 3,5-lut type.

The structure of **2** should be similar to that of the analogous py dimer (**3**)[14] since the 3,5-lut methyl groups are pointing away from Re. The **3**-type structure (see Figure 9 below) readily accounts for the shift pattern. As in the X-ray structure of **3**, the plane of each 3,5-lut is expected to lie in a plane bisecting the *cis* bonds. As a result, half of each stacked 3,5-lut (3,5-lut^s) is stacked with and shielded by the corresponding half of the other 3,5-lut^s. (These halves are close to and related by the C_2-axis passing through the bridging O.) The signals which are most upfield are assigned to this half (Table 2). The other half of each 3,5-lut^s (displaced away from the C_2-axis) is closer to the terminal ligands, explaining the more downfield shift. From the py dimer structure, we expect one half of the terminal 3,5-lut (3,5-lut^t) to lie over the ring of the Re-ligand-partner, 3,5-lut^s. This position leads to an upfield shift of the signals of this half of the 3,5-lut^t. Since this positioning is not so close as that between the two 3,5-lut^s's, the upfield shift is smaller. With the assignments made, we can state that 180° rotation is slightly faster for 3,5-lut^t than for 3,5-lut^s, since the signals of the former are broader at lower temperatures.

(14) Lock, C. J. L.; Turner, G. *Can. J. Chem.* **1978**, *56*, 179−88.

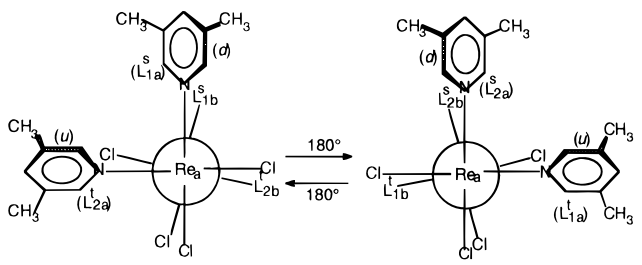

Figure 9. Schematic representation similar to that in Figure 7, with L = a symmetrical pyridine ligand. The rings of only pair 1 are shown to illustrate the relationships of the two halves of each symmetrical ligand going from a stacked site (left) to a terminal site (right).

The presence of all possible EXSY peaks for γ-H, α-H, and β-CH_3 signals in the 2D NOESY/EXSY spectrum at −100 °C (Figure 6) indicates that, even at this low temperature, inversion of chirality and 180° rotation about the Re−N bonds both occur to some extent. The exchange-NOEs in Figure 6 can be grouped into three classes, according to the type of information revealed. One class even reveals which halves of the Re-ligand-partners interchange (Figure 9).

Class (i) exchange-NOEs must result from inversion and reveal little about Re−N rotation. Each γ-H has cross-peaks to all four β-CH_3 signals. Two are direct NOEs between the γ-H and the two β-CH_3. The other two are class (i) exchange-NOEs, arising from the two direct NOEs after the ligand interchanges between t and s sites; these two are expected whether or not 180° Re−N bond rotation is slow or fast.

The α-H signals show direct NOEs to β-CH_3 signals. At low contours, all α-H signals also have two classes of exchange-NOEs. Class (ii) exchange-NOEs indicate only that 180° Re−N rotation is occurring. For example, the downfield α-H of 3,5-lut^s has, in addition to the direct NOE to the signal of the nearby β-CH_3 (downfield 3,5-lut^s β-CH_3 signal), an exchange-NOE to the upfield β-CH_3 signal of 3,5-lut^s. This class (ii) exchange-NOE results from Re−N rotation of 3,5-lut^s. The half of the 3,5-lut^s farther from the C_2-axis is placed closer to the axis by the rotation. Class (iii) exchange-NOEs can be explained only by the inversion of chirality without significant 180° Re−N bond rotation. Examples of this class of exchange-NOE are the cross-peak from the upfield β-CH_3 of 3,5-lut^s to the downfield α-H signal of the 3,5-lut^t and the cross-peak from the upfield α-H of 3,5-lut^s to the downfield β-CH_3 of 3,5-lut^t. These cross-peaks demonstrate that the Re-ligand-partners move in concert with the downfield half of the 3,5-lut^t undergoing physical exchange of position with the upfield half of the 3,5-lut^s. This relationship establishes the exchange process shown in Figure 9 because inversion of chirality interchanges the positions of these halves of the two ligands. Thus, these class (iii) exchange-NOEs demonstrate that the overall net process, rotation about the Re−O−Re bond system and the 90° rotation, is faster than 180° rotation about the Re−N(3,5-lut) bonds.

To aid the discussion, we define the coordination plane (CP); both CP's considered here will contain the ligand's N donor and the *trans* Cl atoms and are thus distinguished by the two other ligating atoms in the CP, namely O═Re−O(bridging) and (*cis*-N)−Re−Cl. Net inversion of chirality for $[Re_2O_3Cl_4L_4]$ dimers with C_2-symmetrical ligands could occur if the ligand plane rotated by ∼90° through either one of these two CP's (Figure 10). The sense of the rotation is different for the two options. The first option, rotation through the O═Re−O CP

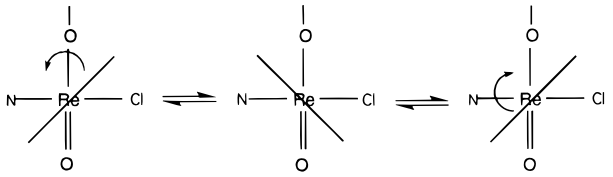

Figure 10. Schematic representation similar to that in Figure 8, but with a symmetrical pyridine-type ligand represented by the line. It is shown that the same form can be obtained by rotation through either CP.

(left side, Figure 10), explains the preferential interchange of the upfield and downfield halves of the 3,5-lut ligands (Figure 9) established by the class (iii) exchange-NOEs for **2**. The second option, rotation through the Cl−Re−N CP (right side, Figure 10), is shown to be less favored by the exchange-NOE data.

The favored sense of rotation reflects the steric barriers L is expected to encounter as it rotates. The Cl groups and the N ligands are much more bulky than the O ligands (the Re complex at the other side of the bridge oxygen is too distant to affect this rotation in the *anti* conformer, see below). The barrier to rotation across this Cl−Re−N CP would be higher. Furthermore, this second option does not hold for lopsided ligands, such as Me_3Bzm, since a different conformer would result if the plane of the ligand rotated past only the CP defined by the Cl−Re−N bonds (Figure 8). In order for **1** to undergo inversion of chirality by this route, each Me_3Bzm would have to cross a Cl−Re−N CP, a O═Re−O CP, and then back across the Cl−Re−N CP. Following this 270° route to achieve a net 90° Re−N rotation (Figure 8) would greatly hinder the inversion rate; the bulky six-membered ring would have to clash severely with the *cis* Me_3Bzm during the last 90° Re−N rotation. Models suggest relatively much less steric hindrance for 90° rotation of the L plane through the O═Re−O CP, especially since the Me_3Bzm five-membered rings are too small to clash.

The most likely route for the inversion of chirality that is consistent with the data for both **1** and **2** and that appears to be sterically feasible in the models involves three distinct types of rotation processes and an unstable intermediate. Thus, in the least hindered inversion pathway (Figure 11), the first process, a net ∼90° Re−O−Re rotation during which the stacked ligands are moved out and away from each other, forms an *anti* conformer with well-separated L's. Next, all four ligands rotate by ∼90° in rapid succession past the respective O═Re−O CP's (Figure 8). Finally there is a second net ∼90° Re−O−Re rotation in the same direction as the first Re−O−Re rotation.

The rates of inversion for **1** and **2** are expected to be similar for the route just described since there should be little difference in hindrance. However, as mentioned above, the pathway involving 270° rotation should proceed much more slowly for **1**. Thus, the rate of inversion is a way to assess the two pathways. Two distinct sets of L signals were apparent by −60 °C for **1** (Figure 3) and −80 °C for **2** (Figure 5), but the shift differences are greater for **1**. A comparison of the coalescence of signals with approximately the same difference in shifts for L^s and L^t suggests that the rate of inversion of chirality for **1** is less than an order of magnitude slower than for **2**. This result, the exchange-NOE data, and examination of models all strongly suggest that the inversion occurs by the less hindered pathway with the L planes rotating by 90° through the O═Re−O CP for both **1** and **2** (Figures 8 and 10).

Conclusions

In octahedral sites in biological systems, lopsided ligands can select among four staggered orientations. Rarely has more than one staggered conformer been identified for any site. In model

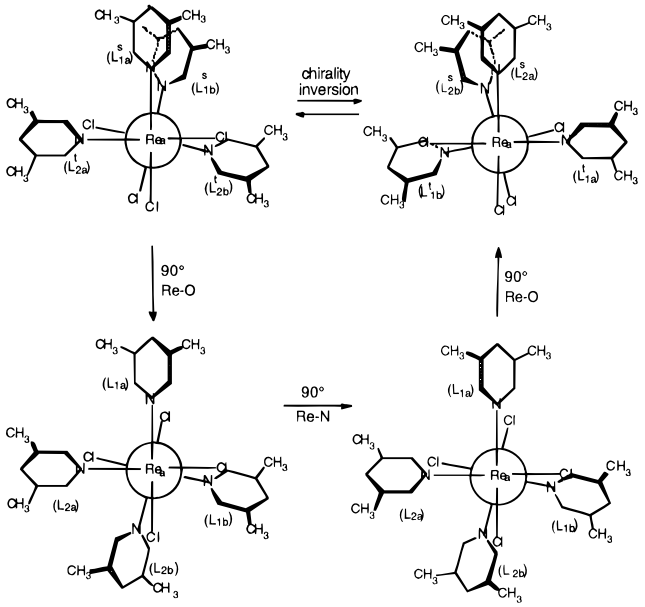

Figure 11. Schematic representation of the complete mechanism proposed for the chirality inversion for **2**. The chirality inversion occurs between the two chiral intermediates with the *anti*-conformation; these are shown at the bottom of the figure.

chiral octahedral complexes, a symmetrical ligand can select between only two possible staggered positions; the ligand can move between the two orientations by two opposing routes of rotation. In this study, we have shown how 2D exchange-NOEs can be used to distinguish these two routes of rotation. To our knowledge, this is the first time preferred pathways of rotation have been demonstrated. Exchange-NOEs have not been widely used to assess dynamic pathways. By comparisons with the analogous complex containing a lopsided ligand, we showed that the lopsided ligand very probably rotates using the same pathway as the symmetrical ligand. Such rotational motion can be significant in many biological processes such as in the formation of DNA cross-links by metal anticancer drugs.

The characteristic HH shift pattern and the NOE data demonstrate that there is only one significant conformer of **1** in solution and that this conformer has the HH,HT,HH structure found in the solid. This is the first case in which the predominant form of a complex with this type of untethered ligand has been shown to be HH in solution. The predominance of this form strongly suggests that the electrostatic attraction of the δ^+ aromatic proton in the imidazole ring of Me_3Bzm^t toward the negative central core of the dimer is responsible for these properties. This conclusion is supported by our studies with Ru^{II} complexes and other Re dimers.[11,12,15]

Acknowledgment. We thank the NIHGMS for support (GM 29222). The instrument purchases were funded by NIH and NSF. NSF (ASC-9527186) supported the use of the Internet for remote collaborative research. L.G.M. was supported in part by Emory's F. M. Bird Exchange Fellowship to St. Andrews University, Scotland.

Supporting Information Available: Crystallographic data for **1**, including tables of positional parameters and bond distances and angles, anisotropic displacement coefficients, H-atom coordinates, view of the packing in *C*2/*c*, and a perspective view of the intermolecular stacking interactions in **1** (19 pages).

JA960385E

(15) Iwamoto, M.; Alessio, E.; Marzilli, L. G. *Inorg. Chem.* **1996**, *35*, 2384−2389.